Journal of Applied Pharmaceutical Science Vol. 13(09), pp 169-189, September, 2023
Available online at http://www.japsonline.com
DOI: 10.7324/JAPS.2023.141546
ISSN 2231-3354

Muntingia calabura Leaves Extracts to Ameliorate chronic obstruction pulmonary diseases by Inhibiting IL-17a Signaling: *In silico* and *in vivo* studies

Nenden Nurhasanah[1], Parichat Phalanisong[2], Fadilah Fadilah[3], Anton Bahtiar[1*]

[1]Department of Pharmacology and Toxicology, Faculty of Pharmacy, Gedung Fakultas Farmasi, Universitas Indonesia, Depok, Indonesia.
[2]SA Interfood and Rice Products Co., Ltd, Khon Kaen, Thailand.
[3]Department of Medicinal Chemistry, Faculty of Medicine, Universitas Indonesia, Jakarta, Indonesia.

ARTICLE HISTORY

Received 22/03/2023
Accepted 30/07/2023
Available Online: 04/09/2023

Key words:
COPD, *Muntingia calabura*, Kersen, IL-17a, *in silico*, TNF-α, COHb.

ABSTRACT

Chronic obstructive pulmonary disease, or COPD, is a disease that commonly breaks the lower respiratory system triggered by continuous exposure to toxic inhalants resulting in oxidative stress accumulation and cascade inflammation process. This disease is one of the top three causes of death in the world. Therapeutic options based on COPD-causing target genes are not currently available. A desired therapeutic candidate acts as an antioxidant and anti-inflammatory and inhibits the expression of COPD-causing related genes. In recent years, using natural compounds as pharmacological therapy has been desirable. Kersen or *Muntingia calabura* is a tropical, evergreen, and fast-growing plant with high anti-inflammatory and antioxidant potential that investigates its effect through molecular analysis upon an *in vivo* COPD model. This study aims to evaluate linking the pathogenesis of COPD and the potential possessed by Kersen leaves and to analyze the mechanism of action of this plant as a therapy for improving COPD conditions. The relationship between the structures of Kersen leaf compounds and COPD was initiated through bioinformatics studies (*in silico*). It was found that the IL-17 signaling pathway is a pathway that Kersen's compounds can intervene against COPD. Molecular docking reveals that quercitrin, myrtillin, and quercetin ligands can bind to IL-17a macromolecules with binding affinity values −7.3, −7.1, and −6.4 kcal/mol, respectively. For the downstream macromolecule, TNF-α successively docked with quercetin, hiravanone, and ononine with −6.7 kcal/mol binding affinity and −5.7 kcal/mol for quercetin. An *in vivo* study used a COPD mouse model combined with cigarette smoke for 14 weeks and Lipopolysaccharides. Meanwhile, Kersen extract started from the 9th week at three different doses, 3.5, 7, and 14 mg per 20 g weight of mice. Kersen's leaves extract at 3.5 mg/20 g weight of mice showed the potential inhibition of cytokine IL-17a, reduced mucus production, and reduced TNF-α expression in the lungs of COPD mice models.

INTRODUCTION

Chronic obstructive pulmonary disease (COPD) is a disease of the lower respiratory system, which can be emphysema and bronchitis, characterized by impaired breathing patterns and limited airflow. The causes of COPD are very complex, involving interactions between genetic factors, cell aging, and continuous exposure to harmful particles, which will disrupt the respiratory system's homeostatic conditions to make morphological changes and functional organ respiration (Hikichi *et al*., 2019). Symptoms seen in COPD patients are shortness of breath, wheezing, chest tightness, and coughing, and they can be accompanied by mucus production, loss of appetite, and weight loss (Wang *et al*., 2020).

COPD ranks as the third leading cause of global death (after ischemia and stroke), with 80% coming from low to middle-income countries. The 2021 Global Initiative for

**Corresponding Author*
Anton Bahtiar, Department of Pharmacology and Toxicology, Faculty of Pharmacy, Gedung Fakultas Farmasi, Universitas Indonesia, Depok, Indonesia.
E-mail: anton.bahtiar @ ui.ac.id

© 2023 Nenden Nurhasanah *et al*. This is an open access article distributed under the terms of the Creative Commons Attribution 4.0 International License (https://creativecommons.org/licenses/by/4.0/).

Chronic Obstructive Lung Disease (GOLD) report states that there are at least 3 million deaths each year due to COPD, with a projected 5.4 million in 2,060 (GOLD Committee, 2021). In Indonesia alone, in 2013, there were 9.3 million people with COPD with various causes, including exposure to air pollution due to industrialization and continuous exposure to cigarettes. 33.8% of Indonesia's population are smokers, including 9.1% of Indonesian teenagers (aged 10–18 years) in 2018.

Current COPD therapy options are still limited, referring to the improvement of symptoms that arise, such as giving bronchodilators (β2 receptor agonists and anti-cholinergic), mucolytics, PDE-4 inhibitors, and glucocorticoids (GOLD Committee, 2021), so there is a need for therapeutic candidates who can provide intervention based on COPD pathogenesis (Wang *et al*., 2020). Various antioxidants can be given as a therapy in COPD management (Hikichi *et al*., 2019).

The potential of Indonesia's biological resources is always interesting to study. One of them, the *Muntingia calabura* plant, known as Kersen, talok, or cherry, is a plant that grows and is easy to cultivate in Southeast Asia, the United States, India, and Brazil (Ansori *et al*., 2021). Kersen is a plant with antioxidants (Rahmawati *et al*., 2018). Biflavans, flavonoids, and dihydrochalcones from the stems of this plant can affect the number of human proinflammatory neutrophils *in vitro* (Kuo *et al*., 2014). The fruit can suppress proinflammatory cytokines (Lin *et al*., 2017). Kersen leaves have cytotoxic activity (Chen *et al*., 2005) and can improve colorectal cancer conditions, regulation of apoptosis, and inflammation (Jisha *et al*., 2020). In addition, Kersen leaves are hepatoprotective (Indriawati, 2020; Rofiee *et al*., 2015; Zakaria *et al*., 2018), antihypercholesterolemia (Ranti *et al*., 2021), gastroprotective (Zakaria *et al*., 2018), antinociceptive (Mohamad *et al*., 2013), and antiproliferative (Desrini and Purnamasari, 2017) and has antimicrobial activity (Buhian *et al*., 2016; Sufian et al., 2013). The main bioactive content that contributes to the pharmacological effects of Kersen is flavonoids (Sari *et al*., 2020), where the value of flavonoids in Kersen leaves is higher than in the stem.

Kersen leaf ethanol extract 6 mg/20-g weight of mice made a difference in alveolar edema, septal destruction, and lung inflammatory cell infiltration of mice exposed to cigarette smoke. Meanwhile, Kersen fruit extract at 100 mg and 200 mg/kg BW can reduce the number of goblet cells in the rat trachea. However, it is not yet known how the molecular mechanism of Kersen can improve the test animals' condition. By linking the pathogenesis of COPD and the potential possessed by Kersen leaves, it is necessary to test and analyze the mechanism of this plant as a therapy for improving COPD conditions, which is the aim of this study.

To predict the possible mechanism of a substance against certain diseases, a bioinformatics approach can be used through network pharmacology and molecular docking, which is then confirmed by *in vitro* or *in vivo* studies (Cao *et al*., 2021). Network pharmacology is a combination of genomic technology and biological systems which, through computational applications, can describe a complex relationship between drug compounds and disease targets by clarifying these relationships through possible mechanisms based on available databases (Sakle *et al*., 2020). The disease targets in the form of genes or proteins (macromolecules) are then tethered with the ligands of the test compounds through molecular docking to determine the affinity and interactions that occur. The conformational change, stability, and interaction mechanism of the tethered protein-ligand complex were then analyzed using molecular dynamics simulations, and *in vivo* analysis using the COPD mice model will be evaluated in this paper.

METHODS

Bioiinformatics studies

Lenovo X1 Carbon laptop, Cytoscape Application 4.2.8, AutoDock Tools 1.5.6, PyRX Screening Tools, Discovery Studios Visualizer v21.1.0.20298, Marvin Sketch are used.

Data collection of Kersen leaf isolates

The 50% ethanol extract from Kersen leaves was taken based on the results of previous studies' gas chromatography/liquid chromathography-mass spectrometry analysis (Pertiwi *et al*., 2020). SMILES structure and canonical information are obtained from the PubChem web server database (https://pubchem.ncbi.nlm.nih.gov/), stored in the spatial data file (SDF) format. The structure was chosen based on the suitability of the formula data (molecular formula) and the compound's molecular weight (exact mass) from the research results.

Drug-likeness analysis

The compounds from the Kersen extract were then assessed for their drug-likeness or potential to be used as medicinal compounds based on their bioavailability value of > 0.17. This information was obtained from shell command file (SCF)Bio-server (http://www.scfbio-iitd.res.in/software/drugdesign/lipinski.jsp#anchortag) and SWISSadme (http://www.swissadme.ch/). Compounds that meet the following criteria will be included in the analysis of protein–protein interactions and molecular docking with the target protein gene.

Target gene data collection

The SMILES canonical data are then used to search for the target genes for each compound. Some of the web-based servers used are SwissPrediction (http://www.swisstargetprediction.ch/), PharmMapper, GeneCards V4.12 (https://www.genecards.org/), Online Mendelian Inheritance in Man (OMIM) (https://omim.org/) Pharmgkb (https://www.pharmgkb.org/) and terapeutic target database (TTD) (http://db.idrblab.net/ttd/) and also (http://www.way2drug.com/passonline/) and Pharmacology Browser 2 (PPB2) https://ppb2.gdb.tools/.

As for the COPD gene, database sources such as PubMed and STRING disease were found in the Cytoscape 3.9.1 application. By using the keyword "chronic obstructive pulmonary disease," you will find COPD genes. The confidence value created is 0.9. In addition, to see the similarity of target genes, you can use DisGeNET (https://www.disgenet.org/search) by typing COPD.

This data collection is in a separate place to facilitate data processing. A list of the target genes is in txt format or excel. If the data are complete, then each network construction is made.

PPI network creation

The entire list of each compound was then collected, and then through the STRING Database in Cytoscape 3.9.1, a retrieving network was carried out with a confidence value of 0.9 to form a target network of Kersen compounds.

The second network, the COPD gene network, was carried out similarly. A list of target genes was collected, and then a retrieving network was carried out with a confidence value of 0.9. The result will form a network of COPD.

Next, carry out the process to create a gene slice that is the same between the compound extract and the COPD network by selecting "tools," then "merge," then selecting the desired network, and selecting "intersection." Then target genes will be found and can be used as therapeutic targets.

Network clusters

Using CytoCluster, the formed network can be grouped into several nearby clusters to facilitate the hypothesis of possible paths. The cluster is assessed based on closeness centrality, degree, closeness centrality, and betweenness values.

Interaction analysis of protein pathway and gene ontology

Analysis of interactions between genes/proteins can be carried out with the help of the STRING platform https://string-db.org/, STITCH http://stitch.embl.de/, and Human References Interactome http://www.interactome-atlas.org/.

The results of the STRING analysis can lead researchers to further analyze the possible pathways as interventions from test substances. Accessible platforms for this analysis include DAVID: Functional Annotation Tools (ncifcrf.gov) and metascape.org and the Kyoto encyclopedia of genes and genomes (KEGG) Pathways database https://-www.genome.jp/.

Virtual screening and molecular docking

Macromolecule and ligand isolate preparation

The ligand and target structures must be prepared in advance. The target macromolecule/protein attached to the complex can be downloaded via the https://www.rcsb.org/ platform. The structure is then prepared by removing water molecules, adding hydrogen atoms, and optimizing amino acids. Meanwhile, the ligand is released and stored in Program database format for grid box optimization in the method validation process. This preparation can be done using the BIOVIA Discovery Studio application.

Validation of the macromolecular method with ligands

The native ligand that had been separated was then re-attached to the macromolecules using the AutoDock 4.0 application.

The appropriate grid box parameter, with a reference value of root mean square deviation (RMSD) < 2 A, will be the benchmark for the next virtual screening.

Virtual screening

We used Vina Wizard on AutoDock 4.0, then entered compounds and macromolecules in pdbqt format. After the process is complete, the binding affinity value and RMSD will appear and can be downloaded. The structure of the isolate, which shows the most negative value in units of kcal/mol and RMSD close to 0, is taken as a compound and then analyzed.

Analysis of docking results with discovery studio

The virtual screening results can be analyzed and visualized using Discovery Studio Visualizer v21.1.0.20298. Several analyses, such as interactions, hydrophobic and hydrophilic bonds, and amino acid residues that bind between proteins/macromolecules and ligands can be carried out.

Molecular dynamics simulation

Molecular dynamics simulations were conducted using GROMACS 2022.2 software with the AMBER99SB-ILDN force field. Electrostatic forces were determined using the Particle Mesh Ewald method. System neutralization was done by adding sodium (Na+) and chloride (Cl−) ions. The solvation stages were carried out using the TIP3P water model. The preparation process for this simulation includes the minimization stage, heating up to 310°K, temperature equilibrium, and pressure equilibrium, and continued with the production process for 100 ns. At the end of the simulation, analysis of RMSD, root mean square fluctuation, radius of gyration (Rg), solvent-accessible surface area, radial distribution function, and hydrogen bond analysis (H) was carried out (−Bond).

***In vivo* studies**

Mice care cages equipped with free access for mice to eat and drink, analytical scales (Ohaus), mice weight scales (Mettler Toledo), Vortex Mixer (Scilogex), Serum Separator Tube (VacuLab), microhematocrit (Marienfeld), surgical instruments (OneMed), Sonde (given intra-gastric), Syringe, UV-Vis Spectrophotometer (Shimadzu 1800), smoking exposure chamber (modification), nebulization kit (Omicron), densitometer, multichannel micropipette, Micropipette, yellow, blue and white tip (Nesco), centrifuge (NUVE NF 048), GEA Freezer (−80°C), Chiller Showcase (GEA), vacuum Rotavapor (Janke and Kunkel IKA, Buchi Rotavapor), glass maceration container, ELISA Microplate Reader (Biochrom EZ), and Freeze dryer (Ihanil Vac 8).

Animals

The animals were male mice (*Mus musculus*) BALB/c strain aged 6–8 weeks weighing about 25–35 g, obtained from PT Biopharma Bandung.

The animals were acclimatized for approximately 7 days, given standard food and drink and sufficient light for 12 hours each in dark and light. The animals are ensured to have access to food and drink freely. Acclimatization was carried out as a process of adapting the mice to the test environment so that the mice were expected not to experience stress during the research. Ethics Committee has approved all protocols, Faculty of Medicine, University of Indonesia with No. KET-583/UN2.F1/ETIK/PPM.00.02/2022.

Sample extracts

Kersen leaves were taken from the Manoko Lembang Medicinal Plants Plantation area, 50% ethanol, and mouse blood

was taken from the orbital sinus, Pulmicort/ budesonide (Actavis), COHb ELISA Kit (Abebio), IL-17A Elisa Kit (Elabscience), water pro injection (Ikapharmindo), aqua dest (PT.Brataco), Ketamine (AgroVet), Xylazim (Interchemie), DjiSamSoe clove cigarettes (tar 39 mg, nicotine 2.3 mg), Quercetin (SIGMA), phosphate buffer saline (PBS) 10× (Sigma Aldrich).

Cigarette exposure system

The smoking-exposure apparatus system uses a glass chamber measuring 45 × 50 × 15 cm to accommodate 12 mice, with air circulation holes on each side of the chamber. The chamber cover uses acrylic material equipped with a small fan to distribute cigarette smoke and move the air. Cigarettes are placed in the socket, where one cigarette produces 36–40 puffs (Hilpert *et al*., 2019).

The mice were exposed to eight cigarettes for 60 minutes, five times a week. Lipopolysaccharides (LPS) was administered intranasally at weeks 1, 3, 5, and 7. At the time of the administration of LPS, the test animals were not exposed to cigarettes. Before administering LPS, mice were given anesthesia using isoflurane 2%, ketamine 80–100 mg/kg, or xylazine 10–12.5 mg/kg intraperitoneal to provide an anesthetic effect for 20–30 minutes.

Exposure to cigarettes was carried out for 8 weeks, where the last 4 weeks of the study were given the test substance 1 hour before exposure to cigarettes.

LPS

LPS of as much as 10 µg dissolved in 30 µl saline was given at weeks 5, 7, 9, and 11.

Preparation of the extracts

Kersen leaf ethanol extract and dosage

Extraction was carried out by maceration using 50% ethanol solvent because several studies showed that 50% ethanol extract of Kersen leaves had total phenolic content, flavonoid values, and high IC50 values (Rahmad et al., 2020).

1 kg of fresh leaves have been dried, then crushed into approximately 800 g of powder. The Kersen leaf powder was then macerated using 50% ethanol 3 times. Extraction is done cold to maintain the content of flavonoids and antioxidant compounds that are susceptible to damage by heat. The filtrate was then concentrated using a 60°C rotavapor until a concentrated liquid extract was obtained, ready to be dried using a freeze-dryer. The results of the yield and calculation of doses can be seen in the appendix.

Lung histological examination

At the end of the study, the animals were sacrificed using an anesthesia procedure by ketamine 80 mg/kg BW and xylazine 50 mg/kg BW. Surgery is performed to take fresh lung tissue. The staining will be carried out using three stainings; they are hematoxylin and eosin (H&E), to evaluate alveolar edema, destruction of the alveolar septum, and infiltration of inflammatory cells in the lung tissue of mice. The second staining is periodic acidic schiff (PAS) to evaluate bronchial wall thickening, goblet cell hyperplasia, and infiltration of interstitial inflammatory cells (Shu *et al*., 2017). The third staining is Masson Trichome staining to evaluate bronchial wall thickening, deposits of collagen fibers, and infiltration of interstitial inflammatory cells (Shu *et al*., 2017).

Mice's lungs were collected and fixed with saline to clean adhering blood and then were placed in a closed tube filled with 10% formalin buffer. The lung tissue was blocked with paraffin, sectioned, and placed on a slide. The slides are then painted with the respective dyes mentioned above. Lung samples were deparaffinized, and tissue was rehydrated using PBS. Then, the slides were dehydrated, cleaned, and covered with a coverslip. This procedure was carried out at the Center for Primate Animal Studies, Bogor Agricultural University.

Bronchoalveolar lavage fluid sampling

Using a 20 g × 1" needle, attach the catheter to the trachea, remove the style hub, make a small hole (incision), and ensure the installation is correct by injecting air through an empty syringe. If the lungs expand, then it is correct. Tie the catheter and trachea together with nylon fibers. Fill a 1 ml syringe with 1 ml cold PBS and place it on the back of the catheter. Gently push the PBS 3 ×, remove the syringe from the catheter, store the liquid in a 1.5 ml Eppendorf (EP) tube, and store it cold. Centrifuge at 10,000 rpm for 10 minutes at 4°C. Transfer the supernatant into a 1.5 ml microtube, then store it at −80°C if the sample is not used immediately (Van Hoecke *et al*., 2017).

Determination of carboxyhemoglobin examination by ELISA

Collect blood from the left/right retro-orbital mice into the serum separator tubes, let it stand for 1.5–2 hours, and then centrifuge it at 5,000 rpm for 10 minutes. Serum sample preparation is listed in the ELISA manual kit (FineTest).

Examination of IL-17A cytokines by ELISA

IL-17a cytokine detection was carried out according to the steps contained in the Kit manual (Elabscience), in which the principle is that the existing plate (well) has been coated with IL-17A antibody (mouse). IL-17A contained in the sample is expected to bind to the antibody in the well. Then, a biotinylated mouse IL-17A antibody was added to bind to the IL-17A present in the sample. Streptavidin-HRP is added and then binds to the biotinylated IL-17A antibody. After streptavidin-HRP was released, washing was carried out; then, the substrate solution was added to form a color depending on the amount of IL-17A in the mice. The reaction will end with the addition of an acidic solution. Absorption is measured at 450 nm.

RESULTS

Analysis of cigarette smokes content by gas chromatography

Gas chromatography-mass spectrophotometry analysis in Table 1 shows that the content of cigarettes used for induction contains nicotine of 15.22%, which can be used to make animal models of COPD through cigarette smoke induction.

The main risk factor for emphysema is smoking. According to clinical data, in Indonesia, there are an estimated 4.8 million COPD patients with a prevalence of 5.6%, of which 90% are smokers (Ministry of Health of the Republic of Indonesia, 2019). Long-term exposure to cigarettes will cause changes in the central lobe of the human lung. In line with animal studies, passive cigarette exposure will produce a pulmonary inflammatory response, especially macrophages. As a result, the bronchial lumen will narrow, the bronchial tissue will be damaged, and even there is rupture and widening of the alveoli so that emphysema is formed (Liang *et al*., 2018).

Flavonoid content

Determination levels of flavonoids are using quercetin as standard. The flavonoid content of ethanolic Kersen extract is 46.05 mg quercetin equivalent/gram or 0.0465% w/b. Other researchers found that the total flavonoid content is 0.06% w/b, equivalent to quercetin/g (Pertiwi *et al*., 2020). The previous study has a few differences in total flavonoid yield, although extraction is done on type plants and the same solvent. The difference in the content metabolites secondary Kersen could be because of different cultivation areas plant as altitude, carbon dioxide level, presence of pests, and species and population of bacteria in the region.

The main bioactive content that contributes to the pharmacological effects of cherries is flavonoids (Sari *et al*., 2020), where the value of flavonoids in Kersen leaves is more than in the stem (Buhian *et al*., 2016).

Table 1. Cigarette smoke content by GC/MS.

No	Compound	RT	Content (%)
1	Caryophyllene	14.407	8.9
2	Nicotine	25.948	15.22
3	Eugenol	38.571	68.54
4	Phenol, 2-methoxy-4-(2-propenyl)-, acetate	39.561	4.43
5	p-Dioxane-2,3-diol	40.139	1.74
6	1,4-Dicyano-2-(5-hexenyl) benzene	41.850	1.17

Analysis of *in silico* bioavailability of Kersen compound

Study-related content extract of 50% ethanol leaves Kersen (Pertiwi *et al*., 2020) shows 42 compounds. Each compound then downloads from *canonical* SMILES, structure two and three dimensions in SDF format using facilities available at PubChem (https://pubchem.ncbi.nlm.nih.gov). The important step in choosing the most suitable structure is matching heavy and formula molecules following LC/GC-MS information to extract 50% ethanol. Each compound is then selected to score its bioavailability through the SwissADME (http://www.swissadme.ch/index.php) and SCFBio (http://www.scfbio-iitd.res.in/software/drugdesign/lipinski.jsp. There are 34 compounds with a bioavailability score of 0.17–0.55, as shown in the table below.

Some of the compounds in Table 2 have been studied for their potential for pathological conditions of the respiratory system, for example, quercetin which can improve lung damage due to cigarette smoke and has entered phase 1 clinical trials (https://ichgcp net/), quercitrin which *in vitro* can inhibit apoptosis and oxidative stress of human bronchial epithelial cells induced by cigarette extracts, arbutin

Table 2. Compound putative extract of Kersen with 50% ethanol with a score bioavailability ≥0.17.

No	Compound	Structure	Molecular weight (g/mol)	*Drug likeliness* value
1	3-Hydroxy-3′,4′-dimethoxyflavone	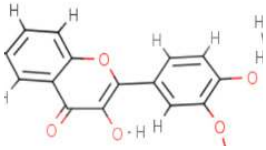	298.29	0.55
2	3,5,8-trihydroxy-7-methoxyflavanone	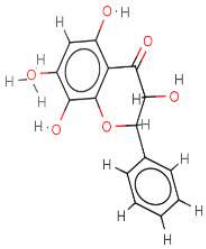	302.28	0.55
3	3’hydroxy-7,8,4′,5′-tetramethoxyflavone/3’-Hydroxy-4′ 5′ ,7,8-tetramethoxyflavone	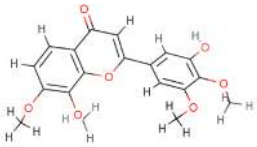	358.3	0.55

Continued

No	Compound	Structure	Molecular weight (g/mol)	*Drug likeliness* value
4	3′-Hydroxydaidzein	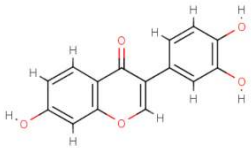	270.24	0.55
5	6-Hydroxyflavanone	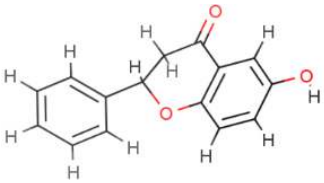	240.25	0.55
6	6,8-diprenyleriodictyol	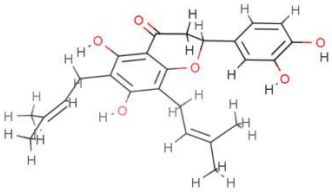	424.49	0.55
7	7,8,3′,4′,5 -Pentamethoxyflavone	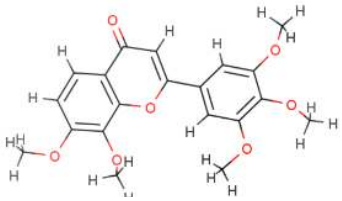	372.37	0.55
8	8,3′-dihydroxy-7,4′,5-trimethoxyflavone	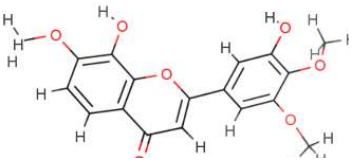	344.3	0.55
9	Arbutin	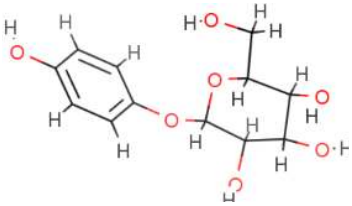	272.25	0.55
10	Catechins	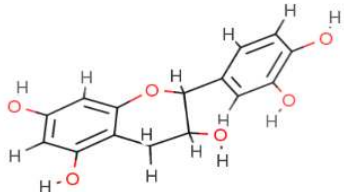	290.07	0.55
11	Cirsiliol	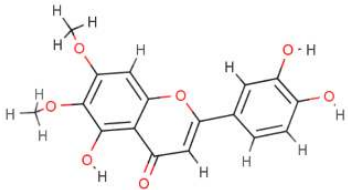	330.29	0.55

Continued

No	Compound	Structure	Molecular weight (g/mol)	*Drug likeliness* value
12	Daidzein	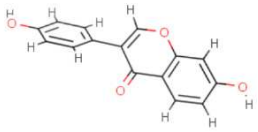	254.24	0.55
13	Dihydrokaempferol		288.25	0.55
14	Epigallocatechin	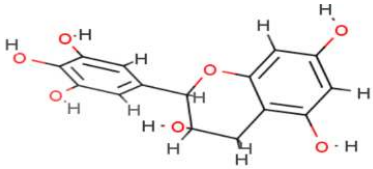	306.27	0.55
15	Epigallocatechin gallate	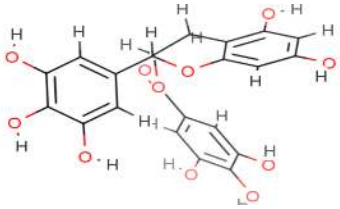	458.4	0.17
16	Formononetin	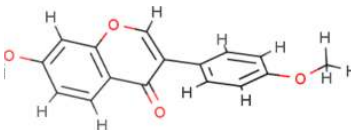	268.26	0.55
17	Gallocatechin	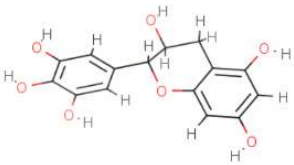	306.27	0.55
18	Geniposide	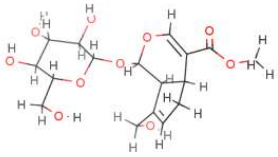	388.37	0.55
19	Hiravanone	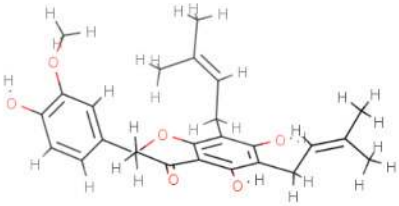	438.5	0.55

Continued

No	Compound	Structure	Molecular weight (g/mol)	*Drug likeliness* value
20	7-Hydroxy flavone	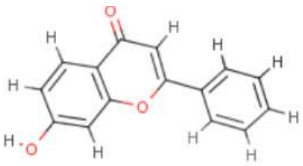	238.24	0.55
21	Isoliquiritigenin	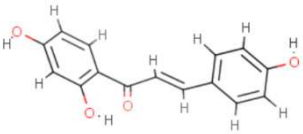	256.25	0.55
22	Kaempferol	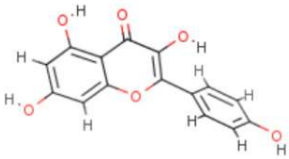	286.24	0.55
23	Kievitone	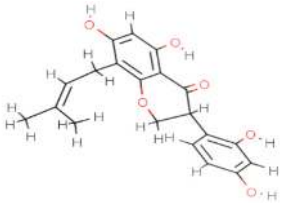	356.4	0.55
24	Lapacho	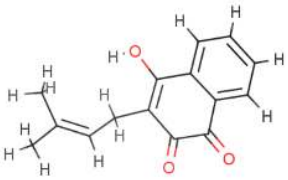	242.27	0.55
25	Myricitrin	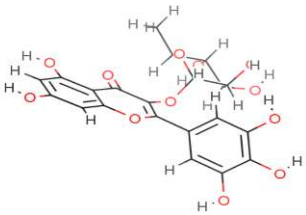	464.4	0.17
26	Myrtillin	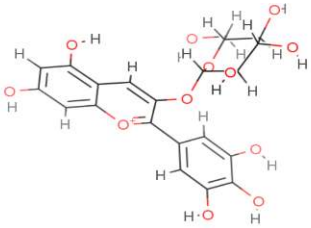	465.4	0.17
27	Narceinone	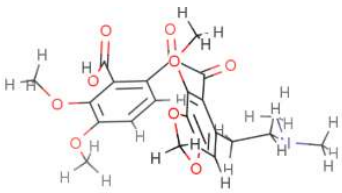	459.4	0.55

Continued

No	Compound	Structure	Molecular weight (g/mol)	*Drug likeliness* value
28	Ononin	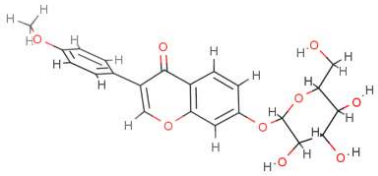	430.4	0.55
29	Quercitrin	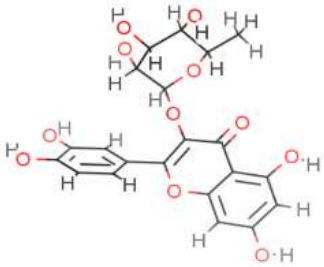	448.4	0.17
30	Quercetin	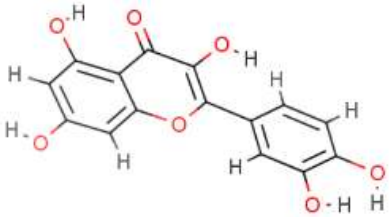	316.26	0.55
31	Rhamnetin	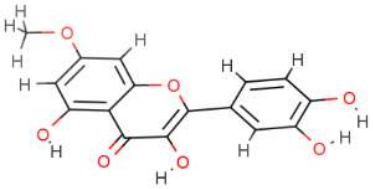	284.22	0.55
32	Rhine	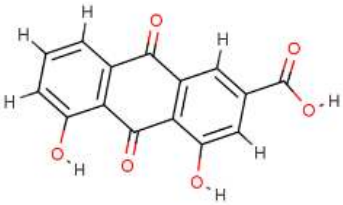	314.29	0.55
33	Velutin	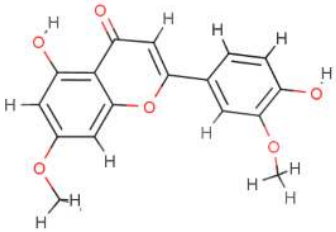	258.27	0.55
34	Yangonin	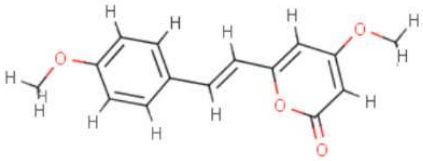	302.23	0.55

Continued

affects mice models of sepsis pneumonia, and LPS-induced, catechin which can improve the symptoms of COPD patients, and epigallocatechin can reduce neutrophilic inflammation and mucus hypersecretion in rats exposed to cigarettes and improve acute lung damage due to *Pseudomonas aeruginosa* (Liang *et al*., 2018).

Results of network protein-protein interaction analysis pharmacology

There are 1,726 associated genes with COPD pathogenesis conditions and 1,132 genes that are the target of the compound Kersen. Several web-based servers are used that is SwissPrediction (http://www.swisstargetprediction.ch/), PharmMapper (http://www.lilab-ecust.cn/pharmmapper/), GeneCards V4.12 (https://www.genecards.org/), OMIM (https://omim.org/) Pharmgkb (**https://www.pharmgkb.org/**), TTD (http://db.idrblab.net/ttd/), (http://www.way2drug.com /passonline/), and PPB2 https://ppb2.gdb.tools/. Retrieval of target genes is carried out on more than one web-based platform because not all compound structures can be identified.

The results of the description of the number of genes involved using https://bioinformatics.psb.ugent.be/webtools/ Venn/ can be seen in the image below:

Figure 1 shows that 423 genes were the same target gene between COPD and Kersen extracts. As many as 32.4% of COPD genes are targets of Kersen compounds, this means Kersen can interfere with the genes involved in COPD. The screening of genes that tend to have a close relationship with one another is based on the values of closeness centrality, degree, closeness centrality, and betweenness values were analyzed. The grouping above uses CytoCluster, the choice of ClusterONE algorithm, then other parameters based on default. Then, several clusters with different confidence values will be formed, so Cluster 5 is chosen, with a *p*-value of 0.001 from the 16 genes below. The thickness of the hexagonal outline in the image above indicates a higher degree value. Here, the TNF gene has a degree value of 14, indicating that the gene is related to other genes in the cluster, as shown in Figure 2.

The results of the analysis of the parameter values of the above genes are shown in Table 3 below.

The topology above can be interpreted as an identification of the role of genes in the network. The degree can be interpreted as whether the gene is directly connected to other genes in the network; closeness centrality is how close the gene is to other genes indirectly. Meanwhile, betweenness centrality describes the gene as the main intermediary between many other nodes/genes in the network.

Gene ontology and pathway analysis

The gene is then analyzed in terms of its enrichment and gene ontology to see the most likely pathways and carried out with the STRING platform https://string-db.org/, DAVID: Functional Annotation Tools (ncifcrf .gov) and metascape.org which is linked to other gene ontology servers such as the genetic association disease database Disease Genetic Association Disease Database (https://geneticassociationdb.nih.gov/) and the KEGG Pathways database https://-www.genome.jp/ and

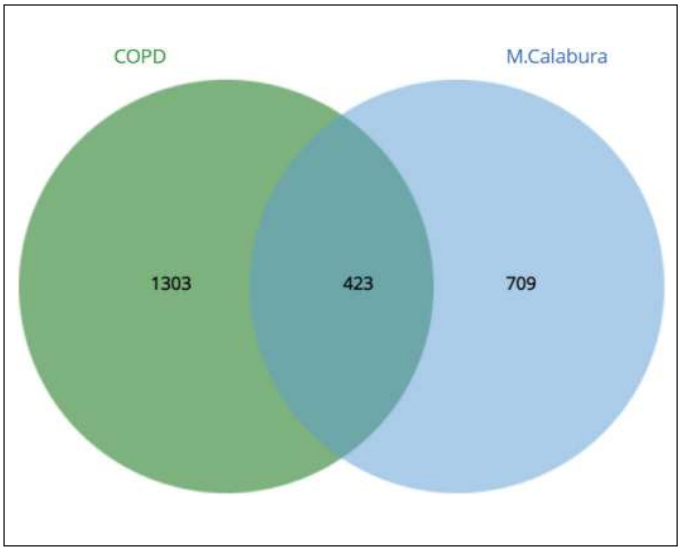

Figure 1. Venn diagram of COPD and Kersen extract target genes.

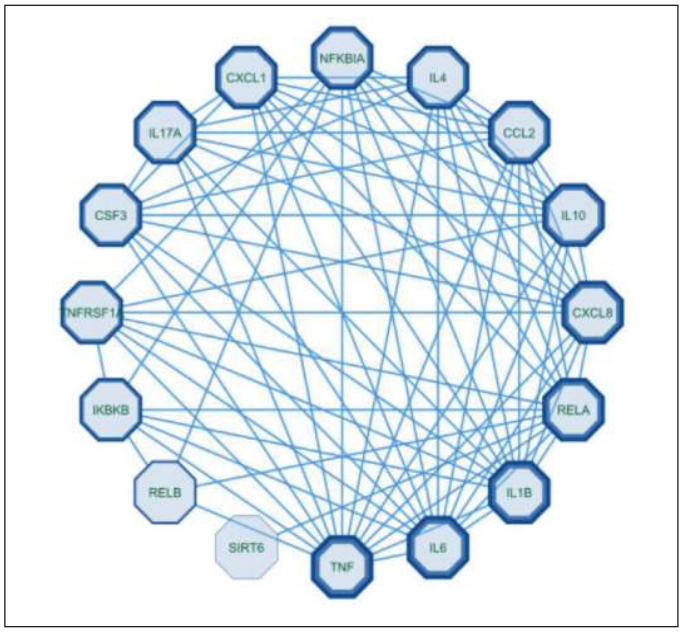

Figure 2. Custer COPD - Kersen target gene.

Human References Interactome http://www.interactome-atlas.org/ as shown in Figure 3.

Figure 4 shows that these genes are genes involved in response to stimuli, in line with the supporting theory that COPD is a disease involving the immune defense in the respiratory system. With consistent exposure to inhaled particles, reactive oxygen species (ROS) and incoming pathogens will be recognized as pattern recognition receptors on the plasma membrane of lung epithelial cells, activating an inflammatory response cascade. If macrophages are activated, these cells will secrete chemokines and cytokines such as tumor necrosis factor-α (TNF-α), which will then induce the expression of adhesion molecules on endothelial cells so that

inflammatory cells can migrate. Macrophages also produce ROS, metalloproteinases (MMPs), and cathepsins, which damage alveolar structures (Hikichi *et al*., 2019).

The abovementioned 16 genes are involved in several signaling pathways, with the result that the IL-17 signaling pathway is ranked first, indicating that this pathway can be used as a referral pathway for analysis of the target mechanism of Kersen extract on the pathogenesis of COPD. In addition to the IL-17 signaling pathway, interleukin signaling, IL-10 signaling, and others are more suggestive of the inflammatory process (Rodrigues *et al*., 2021).

Furthermore, in the picture above, the IL-17 signaling pathway initiates the formation of chemokines and cytokines such as IL-6, CXCL-8, TNF-α, and IL-1β. IL-17a originates from Th17 cells, which are part of effector T cells. Besides producing IL-17a, these cells also produce IL-17f and IL-22. When an infection occurs, these interleukins are needed to eliminate external stimulants, such as bacteria and fungi, by inducing antimicrobial peptides, such as defensins. These cytokines also play an important role in autoimmune and allergic pathogenesis, such as rheumatoid arthritis (RA) (Rodrigues *et al*., 2021).

The receptor that plays a role in the IL-17a signaling pathway in the picture above is IL-17 receptor A (IL-17RA, while the IL-17F receptor is IL-17RC). Currently, four other receptors have been found, namely IL-17RB, IL-17RC, IL-17RD, and IL-17RE (specific receptors for IL-17E, IL-17C, and IL-17F), which have similarities in sequence homology and have a fibronectin III-like domain in the extracellular region and the SEF/IL-17R (SEFIR) domain in the intracellular region. Recent studies have proven that IL-17A and IL-17F are widely expressed in TH17 cells through a heteromeric receptor complex consisting of IL-17RA and IL-17RC, a single transmembrane protein, and are expressed in many places covering various types of cells such as epithelial cells, fibroblasts, and astrocytes (Rodrigues *et al*., 2021).

IL-17 upregulates proinflammatories such as TNF-α, IL-6, G-CSF, IL-1, CXCL1, CCL20, and matrix metalloproteinase through activating the NF-κB, mitogen-activated protein kinases (MAPK), and C/EBP cascades. After IL-17R is activated, the adapter protein Act1 and tumor necrosis factor receptor-associated factor (TRAF) will activate NF-κB. The IL-17R complex recruits act1 through homotypic interactions from the SEFIR domain due to IL-17 stimulation. Furthermore, TRAF6 will be recruited when there is an interaction between Act1 and TRAF so that the TRAF6 task activates downstream TRAF6-dependent TAK1 to activate NF-κB. Act1 mediates in the TRAF6-dependent and TRAF6-independent pathways. In the TRAF6-independent pathway, TRAF2 and TRAF5 are required to induce IL-17 as a stabilizer for CXCL-1 mRNA. The formation of the Act1-TRAF5-TRAF2-SF complex by IL-17 prevents the degradation process if splicing factor binds to CXCL1 mRNA. IKKε directly phosphorylates act1. This phosphorylation is critical for the stabilization of the mRNA cascade. Thus, if candidate compounds can inhibit

Table 3. Kersen-COPD network topology results.

No	Gen	Degrees	Closeness centrality	Stress	Betweenness centrality
1	TNF	14	0.9375	64	0.0851
2	IL6	13	0.8823	44	0.0383
3	IL1B	13	0.8823	44	0.0383
4	WILLING	12	0.83	100	0.17
5	CXCL8	12	0.83	30	0.02
6	CCL2	11	0.78	20	0.01
7	IL10	11	0.75	18	0.02
8	NFKBIA	10	0.75	24	0.01
9	IL4	10	0.75	12	0.0075
10	CXCL1	10	0.75	12	0.0075
11	CSF3	9	0.68	0	0.0056
12	IL17A	9	0.68	0	0
13	TNFRSF1A	8	0.68	8	0
14	IKBKB	7	0.65	6	0.0071
15	RELB	4	0.576	0	0
16	SIRT6	1	0.468	0	0

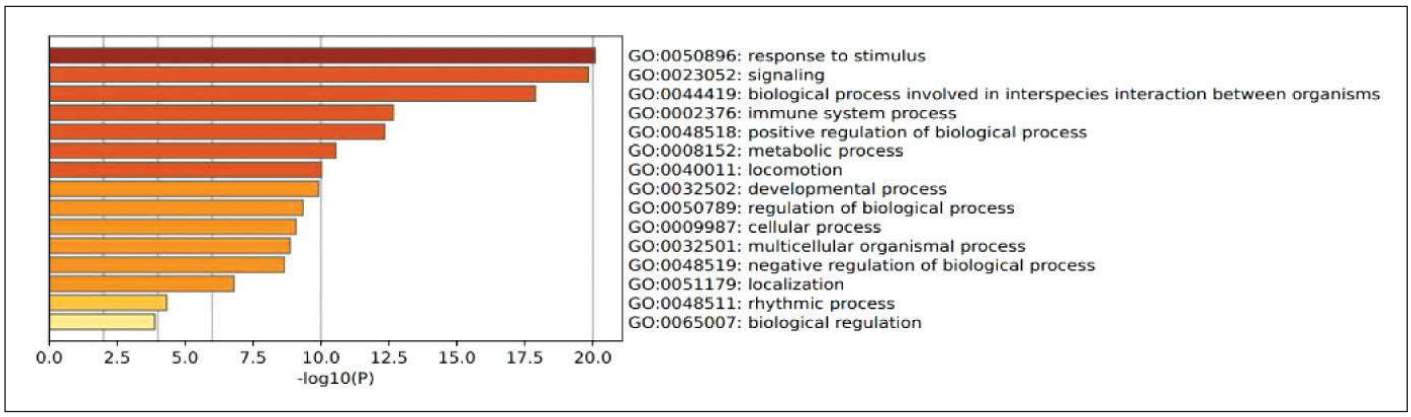

Figure 3. Gene ontology analysis of biological processes between COPD and Kersen target gene.

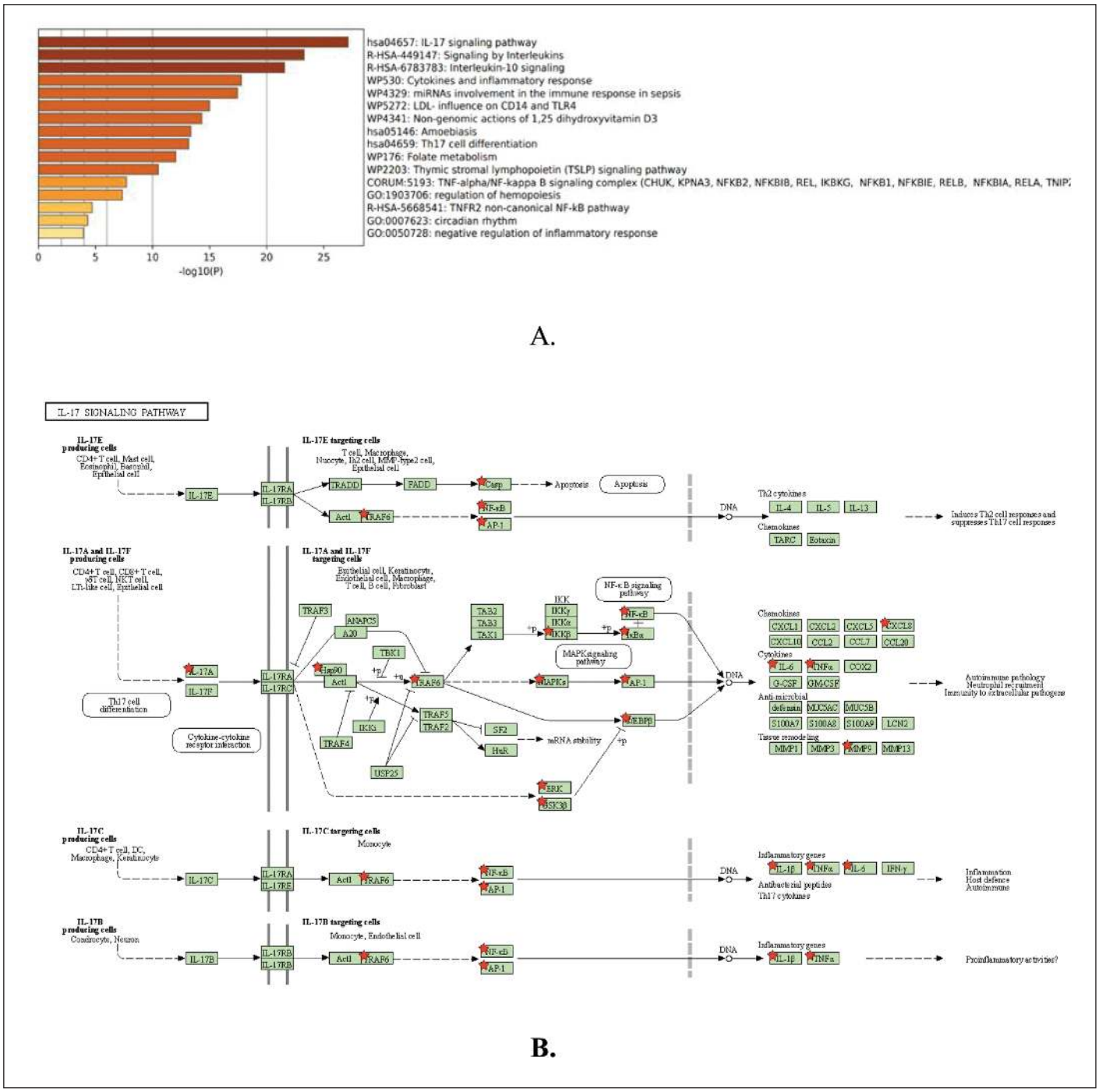

Figure 4. COPD- Kersen signaling pathway. (a) Molecular process pathways. (b) iL-17 signaling pathway.

this pathway, it will prevent the formation of IL-17-mediated disease (Rodrigues *et al*., 2021).

IL-17a originates from Th17 cells, which are part of effector other T cells producing IL-17A cells; it also produces IL-17F and IL-22. Exposure to cigarette smoke could increase work from Th17 to increase mechanism proliferation and apoptosis in cell epithelium channel breath (Montalbano et al., 2015). In addition, smoking is also an adjuvant for Th17 (Chen et al., 2005), signaling IL-17RA will induce MMP12 to support emphysema in tissue. The IL-17A/IL-17 RA axis pathway also plays a role in duct fibrosis breath (Yanagisawa *et al*., 2017).

Molecular docking method validation with AutoDock 4.0

The selected IL-17a macromolecule was 8DYI, with the ligand (5P)-5-[5-(benzylamino)pyridine-3-yl]-N-[2-(morpholin-4-yl)ethyl]-1H-indozole-3- amine (C25H28N6 O) (accessed from: https://www.rcsb.org/). As for TNF-α,

Table 4. The grid box parameters.

Macromolecules	Center			Dimensions (Angstroms)		
	X	Y	Z	X	Y	Z
IL-17A	−49.08	−9.20	9.75	46.64	25	25
TNF-alpha	−19.67	74.01	35.45	29.01	60.02	23.84

Table 5. Conformation best ligand with IL-17a and TNF-**α** macromolecules.

Macromolecules	Compound name	Energy affinity (kcal/mol)	Residue amino acids
IL17-a	Quercitrin	−7.3	Tyr 66, Arg 69, Ser 70, Thr 71, Trp 74, Ile 115, Val 142, Gly 143, Cys 144, Thr 145, Cys 146
	Myritillin	−7.1	Lys 61, Tyr 66, Arg 69, Ser 70, Thr 71, Trp 74, Ile 115, Val 142, Gly 143, Cys 144, Thr 145, Cys 146
	Quercetin	−6.4	Ser 70, Thr 71, Ser 72, Trp 74, Ile 115, Val 142, Gly 143, Thr 145, Cys 144, Cys 146
	(5P)-5-[5-(benzyl amino)pyridin-3-yl]-N-[2-(morpholine-4-yl)ethyl]-1H-indazol-3-amine	−5.24	Gly 29, Ser 30, Ala 31, Met 32, Ala 33, Ser 129
TNF-α	Quercitrin	−6.7	His 15, Leu 57, Ile 58, Tyr 59, Ser 60, Gln 61, Tyr 119, Leu 120, Gly 121, Gly 122, Tyr 151, Ile 155
	Hiravanone	−6.7	His 15, Leu 57, Tyr 59, Ser 60, Gln 61, Tyr 119, Leu 120, Gly 121, Tyr 151, Ile 155
	Ononine	−6.7	Tyr 59, Leu 94, Ala 96, Ile 118, Tyr 119, Leu 120, Gly 121, Tyr 151, Ile 155
	Quercetin	−5.7	His 15, Tyr 59, Ser 60, Gln 61, Leu 120, Tyr 151
	6,7-Dimethyl-3-[(Methyl{2-[Methyl({1-[3-(Trifluoromethyl)phenyl]-1H-indol-3-yl}Methyl) amino]ethyl}amino)methyl]-4H-chromene-4-ONE	−5.58	Arg 44, Val 50, Lys 65, Thr 79

the macromolecule used is 2AZ5 which has the ligand 6,7-dimethyl-3-[(Methyl{2-[Methyl({1-[3-(Trifluoromethyl)) phenyl]-1H-indole-3-yl }Methyl) amino] ethyl} amino) methyl]-4H-chrome-4-ONE. The grid box parameters used after several iterations are listed in Table 4.

Virtual screening with AutoDock Vina

After obtaining the optimal grid size, the parameters obtained are used for the virtual screening process using AutoDock Vina. The results show that quercitrin has the smallest affinity energy for both macromolecules, as shown in Table 5, Figures 5 and 6.

Based on the results of this bioinformatics study, a very potent compound, quercitrin, or another name, quercetin 3-rhamnoside, is a bioflavonoid found in many plants and can be consumed. Quercitrin has a bitter taste with pale yellow crystals. When hydrolyzed, it breaks down into quercetin and rhamnose (Septembre-Malaterre *et al*., 2022).

An *in vitro* study conducted by Yu *et al.* proved that quercitrin could protect human bronchial epithelial cells from apoptosis and oxidative damage in the Nrf2/HO-1/NQO1 pathway and the MAPK/ERK pathway (Sharma *et al*., 2020).

Quercitrin significantly affects platelet aggregation, granule secretion, ROS production, and intracellular calcium mobilization, inhibiting platelet activation in arterial thrombosis. During cell activation, quercitrin inhibits platelet signal transduction mediated by glycoprotein VI, reduces phosphorylation of TNF receptor components, and inhibits FeCl3 induction, which plays a role in thrombus formation (Oh *et al*., 2021).

The molecular docking results above show that quercitrin can bind well with IL-17a and TNF-α with a bond energy affinity of −7.3 and −6.7 kcal/mol, respectively. The type of bond between IL-17a and quercitrin is noncovalent, namely van der Waals bonds on residues Arg 69, Ser 70, Ser 72, Ile 115, Gly 143, Thr 145, and Cys 146 and hydrogen bonds which are located on acidic residues. There are amino Tyr 66, Thr 71, and Cys 144, as well as two bonds on other residues, namely Val 142 and Trp 74. In the TNF-α macromolecule, the noncovalent bonds are van der Waals bonds at residues Gln 61,

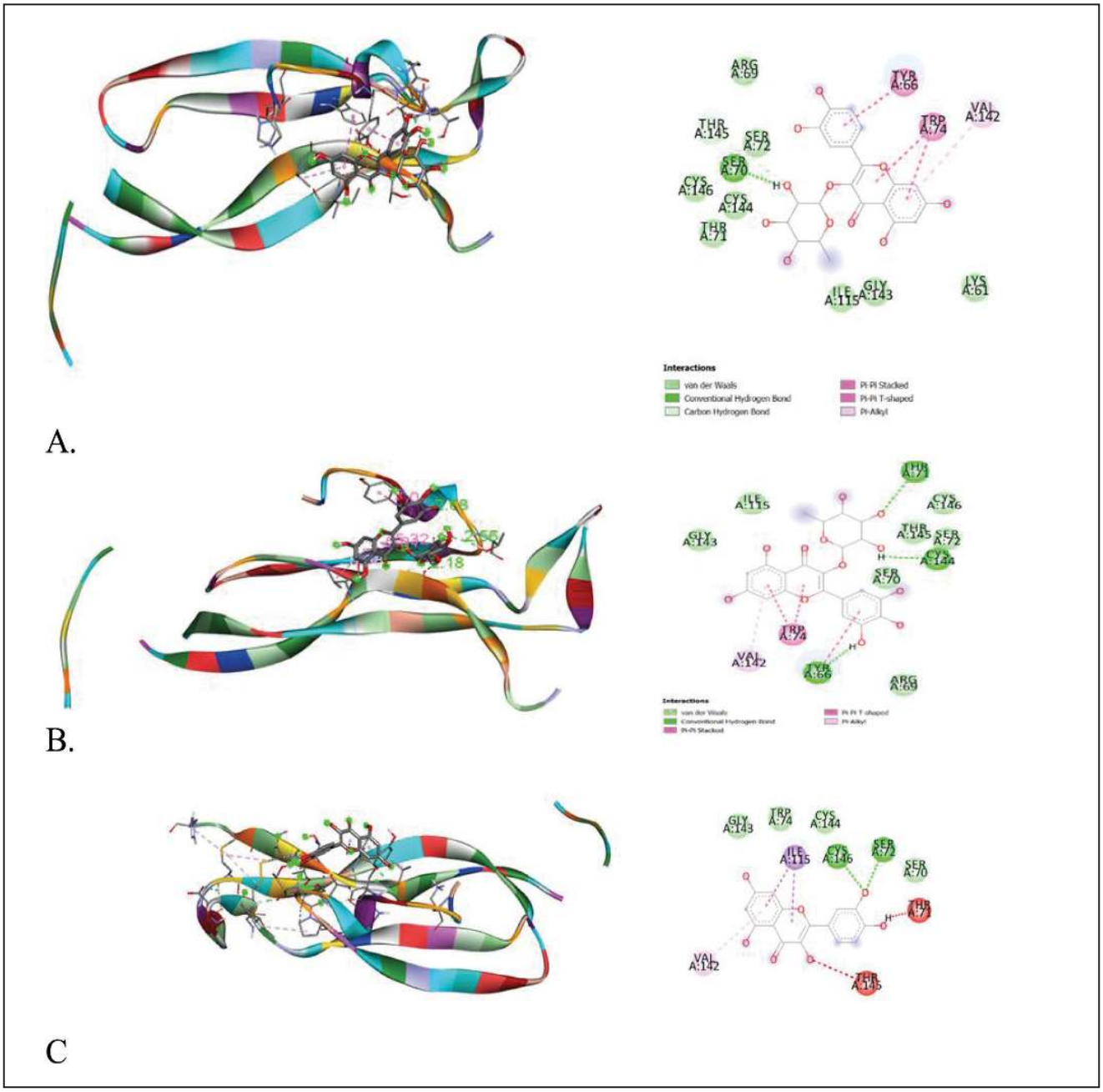

Figure 5. Visualization of binding and attachment sites of compounds with macromolecule IL-17a. (a) Quercitrin. (b) Myrtillin. (c) Quercetin.

Gly 121, Gly 122, and Ile 155. Hydrogen bonding in Ile 58, Leu 120, and Tyr 151. Hydrogen bonding plays a role in stabilizing molecular interactions between ligands and proteins, such as enzyme catalysis, substrate-inhibitor complexes, and the stability of protein structures. Biological molecules are affected by this bond (Kelepouri *et al*., 2018).

Dynamic molecular simulation of IL-17a

Molecular dynamic simulation is a method to describe the stability of a ligand to a macromolecule in its binding pocket by taking into account the side chains, the backbone flexibility of the protein, and the influence of the solvent. Dynamic simulations support optimizing research designs with characteristics relevant to the biomolecular system (Durrant and McCammon, 2011).

To see the prediction of the stability of the bond between quercetin and quercitrin with the IL-17a macromolecule, a dynamic simulation analysis was carried out using Gromacs at a period of 10 ns.

The two RMSD images in Figures 7 and 8 showed that both ligands, quercetin and quercitrin, can bind to the macromolecule IL-17a (RMSD < 2 Å). RMSD is the average movement of atoms

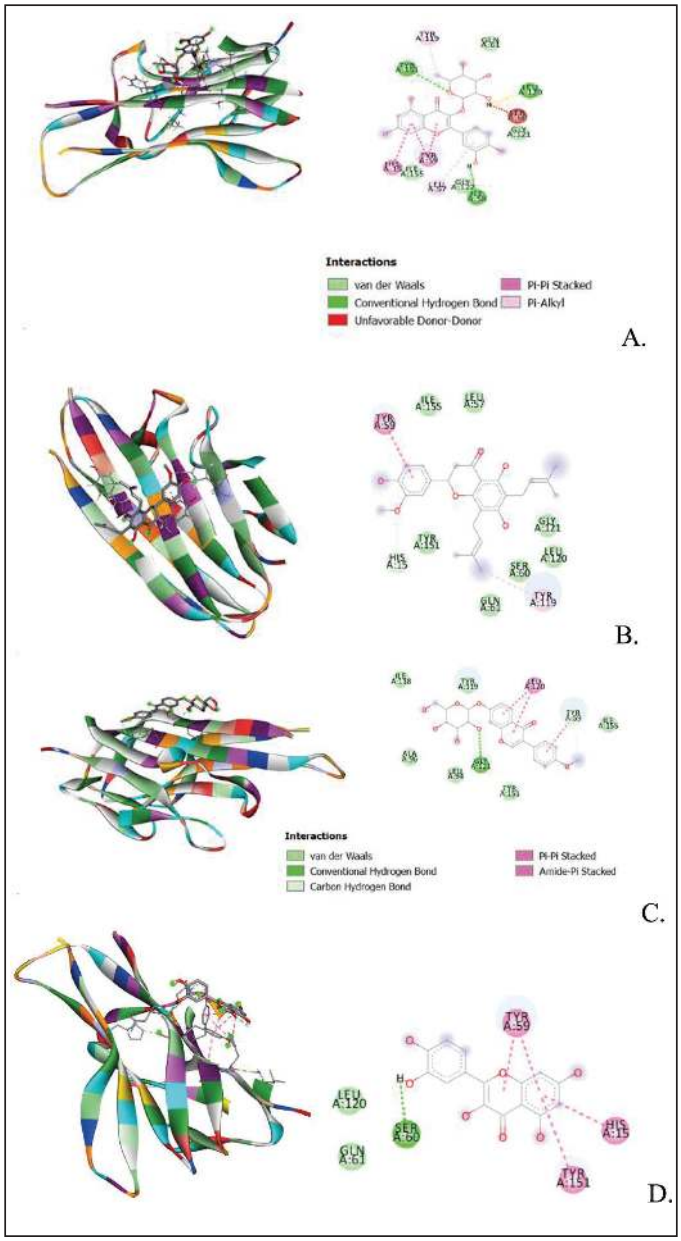

Figure 6. Visualization of binding and attachment sites of compounds with TNF-α macromolecules. (A) Quercitrin. (B) Hiravanone. (C) Ononine. (D) Quercetin.

from one point to another at specific time intervals. In other words, this value indicates the average distance between ligands and macromolecules (Fatriansyah et al., 2022). However, even though the value of the binding affinity energy for molecular quercitrin binding (−7.3 kcal/mol) is better than that of quercetin (−6.4 kcal/mol) when confirmed using dynamic simulations; it appears that quercetin is a more stable binding to the IL-17a ligand, whereas 800ps ligand quercitrin still has fluctuations.

Mice weight monitoring chart

In the first and second weeks, all groups of mice showed normal weight gain. Entering the third week, the group of mice treated with cigarette smoke showed smaller weight

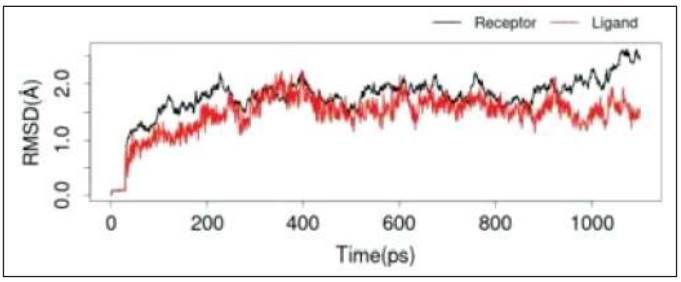

Figure 7. RMSD IL-17a with quercitrin.

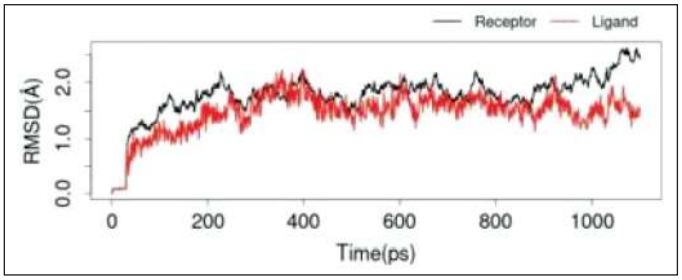

Figure 8. RMSD IL-17a with quercetin.

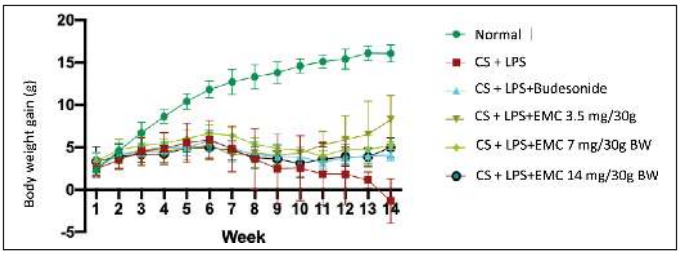

Figure 9. Mice weight monitoring chart.

gain than those not exposed to cigarette smoke. However, this is not due to COPD but because the nicotine in cigarettes can reduce feed intake in mice. Nicotine can affect the hypothalamic melanocortin system, which plays a role in synaptic mechanisms affecting test animals' appetites (Upadhya *et al*., 2020).

The weight chart in Figure 9 shows that the negative group lost weight until the 14th week due to COPD. A Japan cohort study showed that a low body mass index or is associated with an exacerbation process that causes a decrease in FEV1 and the mortality rate of COPD patients. Factors that cause low body mass index include oxidative stress resulting in systemic inflammation, shortness of breath (disruption of the supply of oxygen to cells) and shortness of breath thereby disrupting metabolic rates and reduction of skeletal muscle mass due to an imbalance of oxidants-anti-oxidants which increases muscle proteolysis (Sun *et al.*, 2019).

Exposure to 6–10 cigarettes for 35 days, accompanied by LPS induction, causes weight loss, pulmonary function due to fibrosis, and a low survival rate in mice (Gotts *et al*., 2017).

Evaluation of COHb levels

Table 6 shows that in carboxyhemoglobin levels in the eighth week, cigarette smoke induction can increase the concentration of COHb in the blood. COHb is a complex form

Table 6. COHb concentration after treatment.

Group	Concentration COHb (ppm)
Normal	2.014 ± 0.435
CS + LPS	8.074 ± 2.254
CS + LPS + Budesonide	8.223 ± 1.132
CS + LPS + EMC 3.5 mg/30 g BW	6.202 ± 1.703
CS + LPS + EMC 7 mg/30 g BW	7.001 ± 2.001
CS + LPS + EMC 14 mg/30 g BW	7.774 ± 2.469

Table 7. IL-17a concentration after treatment.

Groups	Concentration IL-17a (pg/ml)
Normal	0 ± 0
CS + LPS	37.125 ± 1.55
CS + LPS + Budesonide 1 mg/BW	23.329 ± 3.93
CS + LPS + EMC 3.5 mg/30 g BW	17.889 ± 4.77
CS + LPS + EMC 7 mg/30 g BW	24.694 ± 3.79
CS + LPS + EMC 14 mg/30 g BW	25.644 ± 3.66

between hemoglobin and carbon monoxide (CO) from exogenous and endogenous sources. The bond between hemoglobin and CO is more stable than that between oxygen and hemoglobin. The presence of CO can come from endogenous and exogenous. Endogenous CO is produced from the enzyme heme oxygenase 1 (HO-1) due to the response of hypoxia, inflammation, and oxidative stress. COHb concentrations can also increase due to the production of proinflammatory cytokines and nitric oxide in the respiratory tract due to viral infections and ROS originating from neutrophils in bacterial infections. This event was also found in patients with asthma and pneumonia, so it can be said that increased COHb is associated with inflammation of the airways and lung parenchyma (Yasuda *et al*., 2005). Exogenous sources of CO come from imperfect oxidation processes of carbon-containing materials, which have a toxic effect because they can act as molecules that can signal apoptosis and oxidative endothelial damage.

The difference in COHb reduction in the extract-treated mice is because 50% Kersen extract acts as an antioxidant (Pertiwi *et al*., 2020), suppressing the oxidation process but only affecting endogenous CO. In this study, exposure to cigarette smoke was still given to all treatment groups so that exogenous CO sources remained. This hypothesis is strengthened by a cohort study proving that baseline COHb levels of smokers were two times higher than nonsmokers, and COHb concentrations increased after smoking (Schimmel *et al*., 2018).

IL-17a cytokine level testing

Table 7 showed that cigarettes and LPS increase IL-17a secretion in line with Montalbaho *et al*.'s research such that cigarettes can increase the stimulation of Th17 cell immunity in COPD patients through the mechanism of proliferation and apoptosis in respiratory epithelial cells (Baskara *et al*., 2020). Then, the role of IL-17 or IL-17a in COPD disease is that it can increase the expression of IL-8 in bronchial epithelial cells (Jan *et al*., 2019) and ADAM-9 in the airways (Li *et al*., 2022). In addition, cigarettes are also an adjuvant for Th17, which through IL-17RA signaling will induce MMP12 to support emphysema in the tissues. The IL-17A/IL-17 RA axis pathway also plays a role in respiratory tract fibrosis (Yanagisawa *et al*., 2017).

HISTOLOGY OF LUNGS

Hematoxylin and eosin stains are the most commonly used staining units. Hematoxylin is not directly used as a dye but requires metal assistance (metal cations such as aluminum) to connect with tissues. The ionic bonds between the tissue and the dye are very important. The hematoxylin will later be positively charged so that it can bind to nucleic acids (negatively charged) to form a blue color. Meanwhile, eosin is an anion that is acidic and negatively charged so that it can bind to positively charged components, such as amino acids, in the cytoplasm to produce a pink color (Wick, 2019).

HE staining measures the degree of inflammation, such as inflammatory cell infiltration, alveolus dissemination, and bronchial wall thickening. The infiltrated inflammatory cells originate from the immune system activation due to cigarette exposure and the induction of LPS, which produces free radicals. Stimulated agents such as macrophages, dendritic cells, and neutrophils stimulate the production of various cytokines, chemokines, protease enzymes, myeloperoxidase, and elastase (Wick, 2019).

The widening of the air cavity due to alveolar damage in COPD conditions is caused by the process of apoptosis in alveolar septal capillary cells, which are very susceptible (Wang *et al*., 2020). Administration of antioxidants can increase α-1antitrypsin, a serine (serine protease inhibitor) that protects the lungs by inhibiting protease-producing neutrophils, thus preventing apoptosis and emphysema (Rangasamy *et al*., 2004). As previously explained, COPD is a manifestation of a protease-anti-protease imbalance, where an excess protease will destroy the alveolar septum, thereby widening the air cavities and reducing the portion of air exchange in the alveoli.

The HE staining on Figure 10 and Table 8 showed that inflammation was significantly different in the Sham group, with the greatest degree in the CS + LPS group (raw data is in the appendix) followed by the CS + LPS + extract *Muntingia calabura* (EMC) 14 mg/30 gBW group (****$p < 0.0001$; *$p < 0.05$). Whereas in the CS + LPS + Budesonide group and CS + LPS + EMC 3.5mg/30gBW, there was a decrease in the degree of inflammation, the cavities between the alveoli were more compact, and the thickness of the bronchial walls decreased and did not differ significantly from the Sham group. That is, administering 50% ethanol extract of Kersen leaves at a dose of 3.5 mg/30 g BW can affect the progression of inflammation in lung tissue. However, in this study, there was no dose-dependent relationship. The higher dose does not show any significant improvement.

PAS staining consists of periodic acid reacted with Schiff's reagent (fuchsin in acid). Periodic acid will oxidize components that have free hydroxyl groups or alkyl amine groups to become dialdehydes. The aldehyde reacts with Schiff's reagent to form an insoluble magenta complex. This magenta complex colors components containing carbohydrates

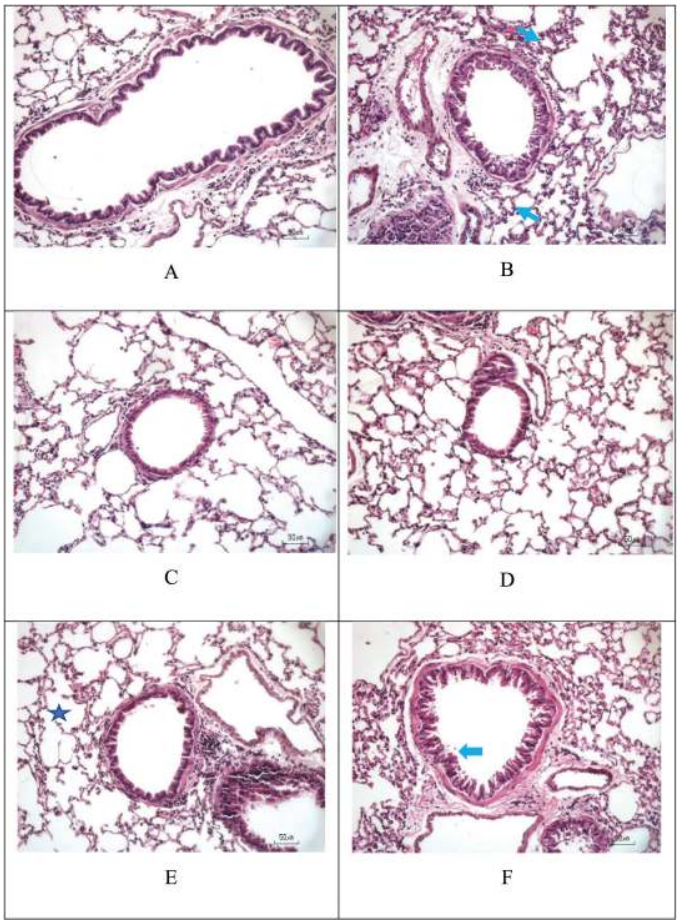

Figure 10. Hematoxylin and eosin staining. Score the degree of inflammation from H&E staining. (A) Sham. (B) CS + LPS. (C) CS + LPS + Budesonide 1 mg/KgBW. (D) CS + LPS + EMC 3.5 mg/30 g BW. (E) CS + LPS + EMC 7 mg/30 g BW. (F) CS + LPS + EMC 14 mg/30 g BW. Scale = 50 µm.

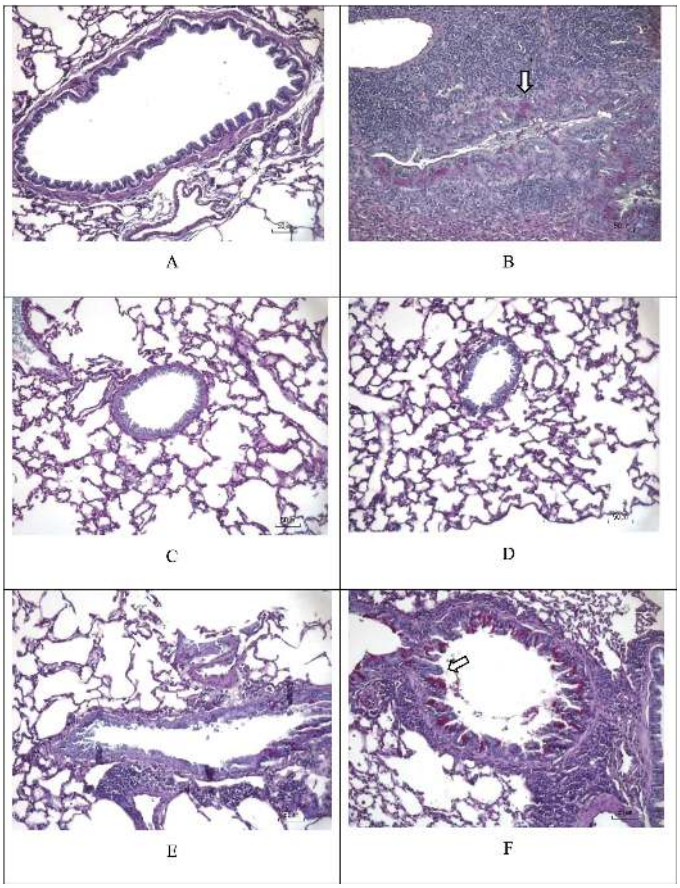

Figure 11. PAS staining. PAS staining to evaluate the presence of mucin-glycoprotein, which is marked with a magenta spot (white arrow). (A) Sham. (B) CS + LPS. (C) CS + LPS+ Budesonide 1 mg/KgBW. (D) CS + LPS + EMC 3.5 mg/30g BW. (E) CS + LPS + EMC 7 mg/30g BW. (F) CS + LPS + EMC 14 mg/30 g BW. Scale = 50 µm.

Table 8. Degree of inflammation hematoxylin and eosin stain.

Group	Inflammation degree ± SD
Normal	1.25 ± 0.63
CS + LPS	3 ± 1.45
CS + LPS + Budesonide 1 mg/BW	2.1 ± 0.91
CS + LPS + EMC 3.5 mg/30 g BW	2.1 ± 0.96
CS + LPS + EMC 7 mg/30 g BW	2.15 ± 1.22
CS + LPS + EMC 14 mg/30 g BW	2.6 ± 1.14

such as glycogen, glycoproteins, and proteoglycans. PAS detects goblet cells and mucin (glycoprotein) in lung tissue in COPD (Hauber and Zabel, 2009).

Mucus is produced by secretory cells, in this case, the goblet cells in the airways function as traps for particles and micro-organisms (these goblet cells are a form of differentiation from epithelial cells). After the mucus task is completed, the trapped mucus and particles will be removed by ciliated cells, commonly called mucous ciliary clearance. However, both of these functions are disrupted in COPD conditions. Overproduction of mucus causes resistance to ciliary movement. Wu *et al.* research proved that cigarette exposure causes epithelial cells to secrete IL-17a, directly stimulating MUC5B expression through the NFκB and Act-1 signaling pathways (Wang *et al*., 2020).

Figure 11 and Table 9 showed components containing glycoprotein were seen in magenta in the CS + LPS group (*$p < 0.05$ for the Sham group) and the CS + LPS group (MCE 7 mg and 14 mg/30 g). Meanwhile, no glycoprotein component was found for the Sham and CS + LPS MCE 3.5 mg/30 g group (#$p < 0.05$ for the CS + LPS group). So it can be said that administering 50% ethanol extract of Kersen leaves at a dose of 3.5 mg/30 g BW can reduce mucus production in COPD conditions. However, in this study, there was no dose-dependent relationship. The higher dose does not show any significant improvement.

Masson's trichrome staining to evaluate the presence of blue (wavy) collagen is shown in Figure 12 and Table 10. The three principles of staining in this staining can stain smooth muscle, collagen fibers, and erythrocytes. In principle, the dye first reacts with acidic components, then when phosphoric acid reacts, components with low permeability/less porous will

Table 9. Mean positive area values of mucin-glycoprotein detection periodic acid Schiff stain.

Group	Mucin glycoprotein ± SEM
Normal	0 ± 0
CS + LPS	2.5 ±0.5
CS + LPS + Budesonide 1 mg/BW	0.25 ± 0.25
CS + LPS + EMC 3.5 mg/30 g BW	0 ± 0
CS + LPS + EMC 7 mg/30 g BW	0.75 ± 0.25
CS + LPS + EMC 14 mg/30 g BW	1.25 ± 0.6

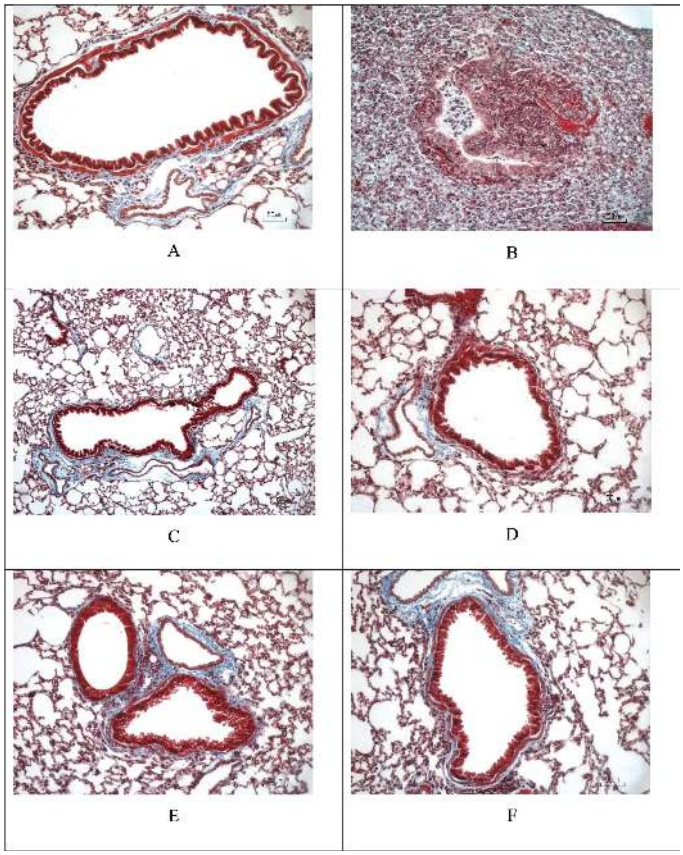

Figure 12. Masson's trichrome staining of cigarette smoke and LPS-induced mice and the treatment. The extent of collagen disposition is indicated by the presence of blue areas in Masson's Trichrome staining. (A) Sham. (B) CS + LPS. (C) CS + LPS + Budesonide 1 mg/KgBW. (D) CS + LPS + EMC 3.5 mg/30 g BW. (E) CS + LPS + EMC 7 mg/30 g BW. (F) CS + LPS + EMC 14 mg/30 g BW. Scale = 50 µm.

turn red, and at the same time, aniline blue enters the collagen component (Bordoloi *et al*., 2020).

The collagen disposition in COPD reflects changes in lung function due to the development of emphysema and mechanical stress around the bronchi. Increased collagen around the alveoli is also caused by damage to parenchymal fibers due to changes in the ratio of collagen type I to collagen type III. The presence of protease activity (MMP-9, MMP13) causes collagen and elastin fibers to become embedded in a shape (Xing *et al*., 2021). Other studies state that in the extracellular

Table 10. Masson's trichrome stain collagen area value.

Group	Collagen area ± SD (µm²)
Normal	1,103 ± 267.1
CS + LPS	3,523 ± 948.5
CS + LPS + Budesonide 1 mg/BW	2,619 ± 1,047
CS + LPS + EMC 3.5 mg/30 g BW	2,418 ± 1,338
CS + LPS + EMC 7 mg/30 g BW	2,801 ± 821.5
CS + LPS + EMC 14 mg/30 g BW	2,013 ± 1,297

matrix, type I and several types IV collagen fragments are degraded by metalloproteinases (MMP) and are associated with the severity of COPD (Calvi *et al*., 2012).

From the above results, it can be seen that at a high EMC dose (14 mg/30 gBW), it gives the smallest collagen area value, followed by a dose of 3.5 mg and then a dose of 7 mg/30 gBW. However, there was no significant difference compared to the CS + LPS group.

The stimulation due to CS + LPS results in acute exacerbations of COPD. In line with research by Yang *et al*. (2021) it was shown that exposure to large areas of collagen in the second and third months increased,.

Evaluation of TNF-α expression by western blotting

TNF-α is known to suppress tropoelastin in lung fibroblasts and regulate MMPs such as MMP-2, MMP-9 which have elastolytic activity, thus preventing MMP overproduction if not inhibited, will cause emphysema characteristics in the lungs (Mukhopadhyay *et al*., 2006).

Previous studies have proven that Kersen fruit *in vitro* using LPS induction can reduce the Expression of TNF-α, IL-1ß, and IL-6 in macrophages through inactivation of the NF-κB pathway, MAPKs p38 and c-Jun NH2-terminal kinase 1/2 (JNK1/2), as well as Janus kinase 2/signal transducers and activators of transcription 1/3, and activation of nuclear factor erythroid-2-related factor 2 (Nrf2) followed by a decrease in the induction of HO-1 production (Lin *et al*., 2017).

TNF-α is a cytokine that is also produced by macrophages. In the IL-17 signaling pathway, IL-17a plays a role in the *de novo* transcription of cytokines, one of which is TNF-α. Figures 13 and 14 showed by western blot analysis, it can be said that the administration of 50% ethanol extract of Kersen leaves can improve COPD characteristics, including parameters of body weight, lung histopathology, and expression of IL-17a and TNF-α in the IL-17 signaling pathway through a model COPD animals, at an optimal dose of 3.5 mg/30 gBW.

The ideal therapy strongly affects the target pathway with minimal effect on other pathways to reduce side effects. Drugs will have pharmacological effects by binding to specific receptors, and the magnitude of the biological response depends on the concentration of the drug-target complex formed (Singh *et al*., 2017). In this study, the concentration at a low dose, namely 3.5 mg/30 gBW, had formed a complex between the receptor and the ligand component of the extract, which, if the concentration were increased, there would be saturation of

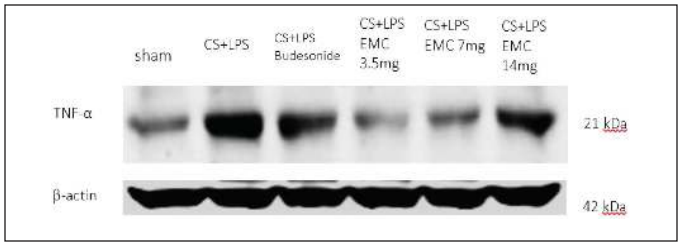

Figure 13. Detection of TNF-α protein level expression from mice lung homogenates.

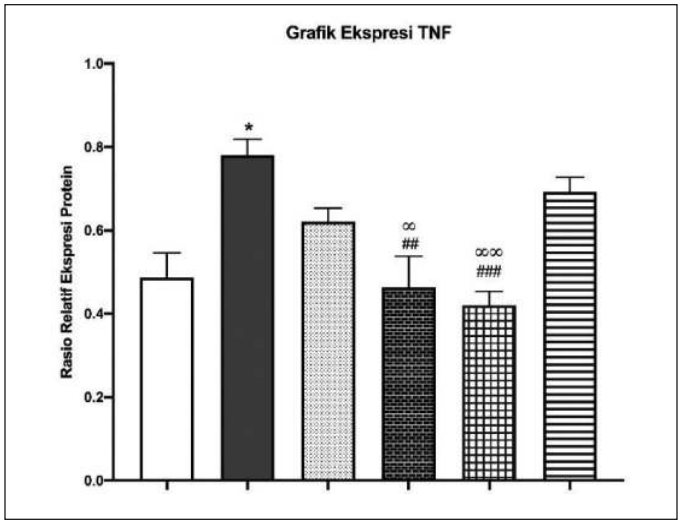

Figure 14. Quantitative TNF-α expression relative to β-actin by ImageJ.

the receptor so that it would not provide improvement in COPD conditions.

There are other possibilities because Kersen extract has cytotoxic activity (Chen *et al*., 2005), so the dose of the extract taken from natural materials with cytotoxic potential can be reduced to get benefits from the extract components. The cytotoxic potential indicates that the components in the extract can be developed into antimicrobial or anticancer agents.

CONCLUSION

Sixteen target genes can be intervened by compounds contained in 50% ethanol extract of Kersen leaves, namely TNF-α, IL6, IL1B, RELA, CXCL8, CCL2, IL10, NFKBIA, IL4, CXCL1, CSF3, IL17A, TNFRSF1A, IKBKB, RELB, and SIRT6.

The content in the 50% ethanol extract of Kersen leaves can intervene in the pathogenesis of COPD in the IL-17 signaling pathway and stably bind to IL-17a for 10ns. So IL-17a (upstream gene) and TNF-α (downstream gene) were selected for *in vivo* confirmation.

Administration of ethanol extract of Kersen leaves can improve COPD characteristics, including weight parameters, lung histopathology, and expression of IL-17a and TNF-α in the IL-17 signaling pathway through COPD animal models at optimal doses of 3.5 mg/30 gBW.

ACKNOWLEDGEMENTS

This research is funded by the Directorate of Research and Development, Universitas Indonesia, under Hibah PUTI 2022 (Grant No. NKB-544/UN2.RST/HKP.05.00/2022).

AUTHORS' CONTRIBUTIONS

AB devised the project and the main conceptual ideas and designed the experiment. FF designed the experiment. NN worked out almost all of the technical details and performed the experiments. NN proposed the experiment in discussions with FF and AB NN, and AB wrote the manuscript.

CONFLICTS OF INTEREST

The authors report no financial or any other conflicts of interest in this work.

ETHICAL APPROVALS

Ethics Committee has approved all protocols, Faculty of Medicine, University of Indonesia with No. KET-583/UN2.F1/ETIK/PPM.00.02/2022

DATA AVAILABILITY

All data generated and analyzed are included in this research article.

PUBLISHER'S NOTE

This journal remains neutral with regard to jurisdictional claims in published institutional affiliation.

REFERENCES

Ansori AN, Kharisma VD, Solikhah TI. Medicinal properties of *Muntingia calabura* l.: a review. Res J Pharm Technol, 2021; 14(8):4509–12; https://doi.org/10.52711/0974-360X.2021.00784

Baskara I, Kerbrat S, Dagouassat M, Nguyen HQ, Guillot-Delost M, Surenaud M, Baillou C, Lemoine FM, Morin D, Boczkowski J, Le Gouvello S. Cigarette smoking induces human CCR6+Th17 lymphocytes senescence and VEGF-A secretion. Sci Rep, 2020; 10(1):6488; https://doi.org/10.1038/s41598-020-63613-4

Bordoloi B, Siddiqui S, Jaiswal R, Tandon A, Jain A, Chaturvedi R. A quantitative and qualitative comparative analysis of collagen fibers to determine the role of connective tissue stroma in oral squamous cell carcinoma using special stains and polarized microscopy. J Oral Maxillofac Pathol, 2020; 24(2):398; https://doi.org/10.4103/jomfp.JOMFP_84_18

Buhian WP, Rubio RO, Valle Jr DL, Martin-Puzon JJ. Bioactive metabolite profiles and antimicrobial activity of ethanolic extracts from *Muntingia calabura* L. leaves and stems. Asian Pac J Trop Biomed, 2016; 6(8):682–85;https://doi.org/10.1016/j.apjtb.2016.06.006

Calvi EN, Nahas FX, Barbosa MV, Calil JA, Ihara SS, Silva Mde S, Franco MF, Ferreira LM. An experimental model for the study of collagen fibers in skeletal muscle. Acta Cir Bras Scielo, 2012; 27(1):681

Cao J, Lei L, Wang K, Sun J, Qiao Y, Duan J, Zhao C, Cui J, Feng Z, Wang JW, Wen A, Yang Z. A network pharmacology approach to predict the proangiogenesis mechanism of huangqi-honghua herb pair after cerebral ischemia. Edited by Nguyen Phuoc Long. Evid Based Complement Alternat Med, 2021; 2021:9834856; https://doi.org/10.1155/2021/9834856

Chen JJ, Lee HH, Duh CY, Chen IS. Cytotoxic chalcones and flavonoids from the leaves of *Muntingia calabura*. Planta Med, 2005; 71(10):970–73; https://doi.org/10.1055/s-2005-871223

Desrini S, Purnamasari D. P1 Antiproliferative and apoptosis induction of methanolic extract from *Muntingia calabura* L leaves on

WiDr colorectal cancer cell line. Biochem Pharmacol, 2017; 139:125; https://doi.org/10.1016/j.bcp.2017.06.002

Durrant JD, McCammon JA.. Molecular dynamics simulations and drug discovery. BMC Biol, 2011; 9(1):71; https://doi.org/10.1186/1741-7007-9-71

GOLD Commitee. GOLD-REPORT-2021-v1.1-25Nov20_WMV.Pdf. 2021. Available via https://goldcopd.org

Gotts JE, Abbott J, Fang X, Yanagisawa H, Takasaka N, Nishimura SL. Cigarette smoke exposure worsens endotoxin-induced lung injury and pulmonary edema in mice. Nicotine Toba Res, 2017; 19(9):1033–39; https://doi.org/10.1093/ntr/ntx062

Hauber HP, Zabel P. PAS staining of bronchoalveolar lavage cells for differential diagnosis of interstitial lung disease. Diagn Pathol, 2009; 4(April):13; https://doi.org/10.1186/1746-1596-4-13

Hikichi M, Mizumura K, Maruoka S, Gon Y. Pathogenesis of chronic obstructive pulmonary disease (COPD) induced by cigarette smoke. J Thorac Dis, 2019; 11(Suppl 17):S2129–40; https://doi.org/10.21037/jtd.2019.10.43

Hilpert M, Ilievski V, Coady M, Andrade-Gutierrez M, Yan B, Chillrud SN, Navas-Acien A, Kleiman NJ. A custom-built low-cost chamber for exposing rodents to e-cigarette aerosol: practical considerations. Inhala Toxicol, 2019; 31(11–12):399–408; https://doi.org/10.1080/08958378.2019.1698678

Van Hoecke L, Job ER, Saelens X, Roose K. Bronchoalveolar lavage of murine lungs to analyze inflammatory cell infiltration. J Vis Exp, 2017; 123:55398; https://doi.org/10.3791/55398

Indriawati, R. The hepatoprotective capacity of steeping Kersen leaves (*Muntingia calabura* l.) on Diabetic Rat. Electron J Gen Med, 2020; 17(5):5–8; https://doi.org/10.29333/ejgm/7888

JLe Jan S, Muller C, Plee J, Durlach A, Bernard P, Antonicelli F. IL-23/IL-17 axis activates IL-1β-associated inflammasome in macrophages and generates an auto-inflammatory response in a subgroup of patients with bullous pemphigoid. Front Immunol, 2019; 10:1972; https://doi.org/10.3389/fimmu.2019.01972

Jisha N, Vysakh A, Vijeesh V, Latha MS. Ethyl acetate fraction of *Muntingia calabura* L. Exerts anti-colorectal cancer potential via regulating apoptotic and inflammatory pathways. J Ethnopharmacol, 2020; 261:113064; https://doi.org/10.1016/j.jep.2020.113064

Kelepouri D, Mavropoulos A, Bogdanos DP, Sakkas LI. The role of flavonoids in inhibiting Th17 responses in inflammatory arthritis. J Immunol Res, 2018; 2018:9324357; https://doi.org/10.1155/2018/9324357

Kirkham S, Kolsum U, Rousseau K, Singh D, Vestbo J, Thornton DJ. MUC5B Is the major mucin in the gel phase of sputum in chronic obstructive pulmonary disease. Am J Respir Crit Care Med, 2008; 178(10):1033–39; https://doi.org/10.1164/rccm.200803-391OC

Kuo WL, Liao HR, Chen JJ. Biflavans, flavonoids, and a dihydrochalcone from the stem wood of *Muntingia calabura* and their inhibitory activities on neutrophil pro-inflammatory responses. Molecules (Basel, Switzerland), 2014; 19(12):20521–35; https://doi.org/10.3390/molecules191220521

Li D, Wang T, Ma Q, Zhou L, Le Y, Rao Y, Jin L, Pei Y, Cheng Y, Huang C, Gai X, Sun Y. IL-17A promotes epithelial ADAM9 expression in cigarette smoke-related COPD. Int J Chron Obstruct Pulmon Dis, 2022; 17:2589–602; https://doi.org/10.2147/COPD.S375006

Liang X, Wang J, Guan R, Zhao L, Li D, Long Z, Yang Q, Xu J, Wang Z, Xie J, Lu W. Limax extract ameliorates cigarette smoke-induced chronic obstructive pulmonary disease in mice. Int Immunopharmacol, 2018; 54:210–0; https://doi.org/10.1016/j.intimp.2017.11.004

Lin JT, Chang YY, Chen YC, Shen BY, Yang DJ. Molecular mechanisms of the effects of the ethanolic extract of *Muntingia calabura* Linn. Fruit on lipopolysaccharide-induced pro-inflammatory mediators in macrophages. Food Funct, 2017; 8(3):1245–53; https://doi.org/10.1039/C6FO01735E

Mohamad Yusof MI, Salleh MZ, Lay Kek T, Ahmat N, Nik Azmin NF, Zakaria ZA. Activity-guided isolation of bioactive constituents with antinociceptive activity from *Muntingia calabura* L. Leaves using the formalin test. Edited by Evan Paul Cherniack. Evid Based Complement Alternat Med, 2013; 2013:715074; https://doi.org/10.1155/2013/715074

Montalbano AM, Riccobono L, Siena L, Chiappara G, Di Sano C, Anzalone G, Gagliardo R, Ricciardolo FLM, Sorbello V, Pipitone L, Vitulo P, Profita M. Cigarette smoke affects IL-17A, IL-17F and IL-17 receptor expression in the lung tissue: *ex vivo* and *in vitro* studies. Cytokine, 2015; 76(2):391–402. https://doi.org/10.1016/j.cyto.2015.07.013

Mukhopadhyay S, Hoidal JR, Mukherjee TK. Role of TNFα in pulmonary pathophysiology. Respir Res, 2006; 7(1):125; https://doi.org/10.1186/1465-9921-7-125

Oh TW, Do HJ, Jeon JH, Kim K. Quercitrin inhibits platelet activation in arterial thrombosis. Phytomedicine, 2021; 80:153363; https://doi.org/10.1016/j.phymed.2020.153363

Pertiwi RD, Suwaldi MR, Setyowati EP. Radical scavenging activity and quercetin content of *Muntingia calabura* L. leaves extracted by various ethanol concentration. J Food Pharm Sci, 2020; 8(1):174–84; https://doi.org/10.22146/jfps.581

Narasati S, Nugroho E, Witjaksono D, Lestari DI, Nugroho MB, Rachmawati S, Ridwan M. The role of pulmonary rehabilitation in acute exacerbations of chronic obstructive pulmonary disease. Int J Appl Pharm, 2020; 12(3 SE-Full Proceeding Paper):39–40; https://doi.org/10.22159/ijap.2020.v12s3.39466

Rahmawati AN, Astirin OP, Pangastuti A. Intracellular antioxidant activity of *Muntingia calabura* leaves methanolic extract. Nus Biosci, 2018; 10(4):210–14; https://doi.org/10.13057/nusbiosci/n100402

Rangasamy T, Cho CY, Thimmulappa RK, Zhen L, Srisuma SS, Kensler TW, Yamamoto M, Petrache I, Tuder RM, Biswal S. Genetic ablation of Nrf2 enhances susceptibility to cigarette smoke-induced emphysema in mice. J Clin Invest, 2004; 114(9):1248–59; https://doi.org/10.1172/JCI21146

Ranti I, Vickasari N, Pangestika SM, Aryani D. Kersen (*Muntingia calabura* L.) leaves extract as a novel alternative therapy for hypercholesterolemia. E3S Web Conf, 2021; 316:03022; https://doi.org/10.1051/e3sconf/202131603022

Rodrigues SD, Cunha CM, Soares GM, Silva PL, Silva AR, Gonçalves-de-Albuquerque CF. Mechanisms, pathophysiology and currently proposed treatments of chronic obstructive pulmonary disease. Pharma (Basel, Switzerland), 2021; 14 (10):979; https://doi.org/10.3390/ph14100979

Rofiee MS, Yusof MI, Abdul Hisam EE, Bannur Z, Zakaria ZA, Somchit MN, Teh LK, Salleh MZ. Isolating the metabolic pathways involved in the hepatoprotective effect of *Muntingia calabura* against CCl4-induced liver injury using LC/MS Q-TOF. J Ethnopharmacol, 2015; 166:109–8; https://doi.org/10.1016/j.jep.2015.03.016

Sakle NS, More SA, Mokale SN. 2020. A network pharmacology-based approach to explore potential targets of caesalpinia pulcherima: an updated prototype in drug discovery. Sci Rep, 2020; 10(1):17217; https://doi.org/10.1038/s41598-020-74251-1

Sari SA, Ernita M, Mara MN, AR MR. Identification of active compounds on *Muntingia calabura* L. leaves using different polarity solvents. Indones J Chem Sci Technol, 2020; 3(1):1–7.

Schimmel J, George N, Schwarz J, Yousif S, Suner S, Hack JB. Carboxyhemoglobin levels induced by cigarette smoking outdoors in smokers. J Med Toxicol, 2018; 14 (1):68–73; https://doi.org/10.1007/s13181-017-0645-1

Septembre-Malaterre A, Boumendjel A, Seteyen AS, Boina C, Gasque P, Guiraud P, Sélambarom J. Focus on the high therapeutic potentials of quercetin and its derivatives. Phytomed Plus, 2022; 2(1):100220; https://doi.org/10.1016/j.phyplu.2022.100220

Sharma A, Parikh M, Shah H, Gandhi T. Modulation of Nrf2 by quercetin in doxorubicin-treated rats. Heliyon, 2020; 6(4):e03803; https://doi.org/10.1016/j.heliyon.2020.e03803

Shu J, Li D, Ouyang H, Huang J, Long Z, Liang Z, Chen Y, Chen Y, Zheng Q, Kuang M, Tang H, Wang J, Lu W. Comparison and evaluation of two different methods to establish the cigarette smoke exposure mouse model of COPD. Sci Rep, 2017; 7(1):15454; https://doi.org/10.1038/s41598-017-15685-y

Singh R, Iye S, Prasad S, Deshmukh N, Gupta U, Zanje A, Patil S, Joshi S. Phytochemical analysis of *Muntingia calabura* extracts possessing antimicrobial and anti-fouling activities. Int J Pharma Phytochem Res, 2017; 9:826–32; https://doi.org/10.25258/phyto.v9i6.8186

Sufian AS, Ramasamy K, Ahmat N, Zakaria ZA, Yusof MI. Isolation and identification of antibacterial and cytotoxic compounds from the leaves of *Muntingia calabura* L. J Ethnopharmacol, 2013; 146(1):198–204; https://doi.org/10.1016/j.jep.2012.12.032

Sun Y, Milne S, Jaw JE, Yang CX, Xu F, Li X, Obeidat M, Sin DD. BMI Is associated with FEV(1) decline in chronic obstructive pulmonary disease: a meta-analysis of clinical trials. Respir Res, 2019; 20(1):236; https://doi.org/10.1186/s12931-019-1209-5

Upadhya MA, Upadhya HM, Borkar CD, Choudhary AG, Singh U, Chavan P, Sakharkar A, Singru P, Subhedar NK, Kokare DM. Melanocortin-4 receptors modulate nicotine-induced brain stimulation reward in ovariectomized rats. Neuroscience, 2020; 431:205–21; https://doi.org/10.1016/j.neuroscience.2020.01.035

Wang C, Zhou J, Wang J, Li S, Fukunaga A, Yodoi J, Tian H. Progress in the mechanism and targeted drug therapy for COPD. Signal Transduct Target Ther, 2020; 5(1):248; https://doi.org/10.1038/s41392-020-00345-x

Wick MR. The hematoxylin and eosin stain in anatomic pathology—an often-neglected focus of quality assurance in the laboratory. Semin Diagn Pathol, 2019; 36(5):303–11; https://doi.org/10.1053/j.semdp.2019.06.003

Wu D, Jiang W, Liu C, Liu L, Li F, Ma X, Pan L, Liu C, Qu X, Liu H, Qin X, Xiang Y. CTNNAL1 participates in the regulation of mucus overproduction in HDM-induced asthma mouse model through the YAP-ROCK2 pathway. J Cell Mol Med, 2022; 26:1656–71. https://doi.org/10.1111/jcmm.17206

Xing T, Zhao ZR, Zhao X, Xu XL, Zhang L, Gao F. Enhanced transforming growth factor-beta signaling and fibrosis in the pectoralis major muscle of broiler chickens affected by wooden breast myopathy. Poult Sci, 2021; 100(3):100804; https://doi.org/10.1016/j.psj.2020.10.058

Yanagisawa H, Hashimoto M, Minagawa S, Takasaka N, Ma R, Moermans C, Ito S, Araya J, Budelsky A, Goodsell A, Baron JL, Nishimura SL. Role of IL-17A in murine models of COPD airway disease. Am J Physiol Lung Cell Mol Physiol, 2017; 312 (1):L122–30; https://doi.org/10.1152/ajplung.00301.2016

Yang Y, Di T, Zhang Z, Liu J, Fu C, Wu Y, Bian T.. Dynamic evolution of emphysema and airway remodeling in two mouse models of COPD. BMC Pulm Med, 2021; 21(1):134; https://doi.org/10.1186/s12890-021-01456-z

Yasuda H, Yamaya M, Nakayama K, Ebihara S, Sasaki T, Okinaga S, Inoue D, Asada M, Nemoto M, Sasaki H. Increased arterial carboxyhemoglobin concentrations in chronic obstructive pulmonary disease. Am J Respir Crit Care Med, 2005; 1711246–51; https://doi.org/10.1164/rccm.200407-914OC

Yu D, Wang F, Ye S, Yang S, Yu N, Zhou X, Zhang N. Quercitrin protects human bronchial epithelial cells from oxidative damage. Open Med (Warsaw, Poland), 2022; 17(1):375–83. https://doi.org/10.1515/med-2022-0416

Zakaria ZA, Mahmood ND, Mamat SS, Nasir N, Omar MH. Endogenous antioxidant and LOX-mediated systems contribute to the hepatoprotective activity of aqueous partition of methanol extract of *Muntingia calabura L.* Leaves against paracetamol intoxication. Front Pharmacol, 2018; 8:982; https://doi.org/10.3389/fphar.2017.00982

How to cite this article:
Nurhasanah N, Phalanisong P, Fadilah F, Bahtiar A. *Muntingia calabura* leaves extracts to ameliorate Cchronic Oobstruction Ppulmonary Ddiseases by inhibiting IL-17a signaling: *iIn- silico* and *in- vivo* studies. J Appl Pharm Sci, 2023; 13(09):169–189.